Analyst

PAPER

View Article Online
View Journal | View Issue

Cite this: *Analyst*, 2026, **151**, 2037

Continuous monitoring of glutamate using electroactive templated polymers as synthetic molecular receptors

Samin Motallebzadeh,[a] Leila Ahmadian-Alam,[b] Masoumeh Bahrami,[a] Arturo Andrade[c,d] and Edward Song *[a]

Received 15th October 2025,
Accepted 20th February 2026

DOI: 10.1039/d5an01088h

rsc.li/analyst

Selective and spatiotemporally resolved monitoring of glutamate in the brain is essential for understanding its role in many brain functions as well as in the progression of various mental disorders. However, achieving accurate time resolved glutamate detection has been challenging due in part to the lack of glutamate-binding receptors that can offer both target selectivity and continuous measurement capability. To address this challenge, we have developed a novel polymer-based electrochemical biosensor designed to enhance selectivity for glutamate. Our proposed biosensor incorporates an innovative templated polymer-based target receptor, which selectively binds to the glutamate molecule. Furthermore, the reversible binding kinetics enable continuous glutamate detection with a time resolution of approximately 1 minute and a detection limit of 88.5 nM in artificial cerebrospinal fluid (ACSF) buffer. Additionally, due to the synthetic target-imprinted receptors, the sensor exhibited high selectivity for glutamate in the presence of other interfering neurochemicals GABA, glycine, and aspartate. These results indicate that the proposed sensor technology holds potential for monitoring glutamate in real physiological samples with possible use in clinical settings.

1. Introduction

Glutamate (Glu) is the most abundant excitatory neurotransmitter in human brain, and its signaling participates in a wide range of brain functions including learning, memory formation, long-term potentiation and synaptic plasticity.[1–5] Recent studies suggest that malfunction in glutamatergic signaling has pervasive implications in many neurological and neurodegenerative disorders such as epilepsy,[6,7] Alzheimer's disease,[8–11] Parkinson's disease,[12,13] Schizophrenia,[14–16] and even in drug addiction[17,18] and cancer progression.[19,20] Therefore, accurate and reliable monitoring of Glu is essential for understanding the various mechanics of Glu transmission and their functionalities at the cellular level as well as their impacts on mental health conditions.

Currently, Glu measurement in brain tissue is done in several methods. A whole-cell patch clamp is the gold standard technique for electrophysiology studies.[21–23] Patch clamp interprets glutamatergic synaptic transmission by monitoring electrical changes that result as a consequence of the activation of ionotropic receptors to glutamate. Although it has the fastest time resolution (milliseconds), this technique lacks chemical selectivity and difficulty in spatial mapping in the extracellular space. Genetically encoded optical Glu sensors such as iGluSnFR are able to map Glu activities in large area with excellent spatiotemporal resolution,[24–27] however imaging is limited to regions expressed with fluorescence-labeled proteins which are typically the cell membrane and the intracellular regions making it difficult to measure Glu in the extracellular regions. Microdialysis offers highly accurate detection of extracellular Glu in terms of chemical specificity and quantification, however, this method has relatively low time resolution (on the order of minutes) and lacks spatial mapping capability. Enzymatic biosensors are highly effective in measuring extracellular Glu,[28–30] however, the downside is ensuring stability in enzyme activities during measurements for reliable long term monitoring as well as difficulty in achieving multi-analyte detections.[31] Therefore, there is a critical need for the development of a new sensing technology that is reliable, selective, and can be miniaturized to achieve Glu mapping in tissue samples with high spatial and temporal resolution.

Electrochemical sensing is a promising tool in neurochemical monitoring due to its fast response time and its ease of

[a]*Department of Electrical & Computer Engineering, University of New Hampshire, Durham, NH 03824, USA. E-mail: Edward.Song@unh.edu*
[b]*Flexcon Company, Inc., Spencer, MA 01562, USA*
[c]*Department of Neuroscience, Brown University, Providence, RI 02912, USA*
[d]*Robert J. & Nancy D. Carney Institute for Brain Science, Brown University, Providence, RI 02912, USA*

miniaturization. Although electrochemical sensors have been successful in measuring electroactive neurochemicals (*e.g.*, dopamine and serotonin) with high spatiotemporal resolution,[32–34] non-electroactive species, such as glutamate and gamma-aminobutyric acid (GABA), have been difficult to measure because they do not easily oxidize or reduce to give electrochemical responses. Recently, there has been a great interest in developing non-enzymatic electrochemical sensors to address the challenges associated with enzymatic Glu sensors.[35] Recently, the author's team has developed a new electrochemical sensing platform that can detect non-electroactive neurochemicals using a polymer-based synthetic target receptors that can achieve rapid response time (Fig. 1).[36–38] Our sensor platform is based on a linear chain stimuli responsive polymer that exhibits high affinity toward the target molecule with which the polymer is templated. Furthermore, upon target recognition, the polymer undergoes conformation change between folded/collapsed and unfolded/open morphologies. This conformation change upon specific target recognition is due to the use of a stimuli-responsive polymer that has the actuation capability upon a stimulus input (*i.e.*, target binding). Also, since each receptor is made up of a single linear polymer chain without any interchain cross-linkers, the proposed polymer architecture allows target molecules to easily access the binding sites thereby promoting rapid response time. This polymer-based target recognition approach is similar in concept to, and has been partially inspired by, the electrochemical aptamer-based sensors.[39–43] However, while aptamers are highly effective in detecting large molecular weight targets (*e.g.*, proteins and drugs), creating high performance aptamers for small molecules such as Glu has been challenging.[44] Moreover, the proposed templated polymer's simplistic molecular structure, compared to aptamers, makes it effective in interacting with small molecule neurotransmitters such as glutamate. This technology complements and further strengthens the aptamer-based sensors by providing an additional library of synthetic receptors for small molecules that are currently difficult to monitor in real-time. In summary, the key innovation of our proposed sensing technology is in the use of the self-actuating polymers that are directly templated with the analyte molecule for enhanced target selectivity, combined with their capability to achieve label-free detection due to the folding and unfolding of the polymer induced by the target recognition (*i.e.*, target binding). Therefore, this sensing platform further expands our capability, beyond aptamer-based biosensors, to achieve continuous and real-time detection using electrochemical sensing technique in combination with shape-changing target receptors.

In our previous work,[38] we have shown that by incorporating redox-active osmium complex as a redox label into the polymer chain, the conformation changes of the target receptor could be detected by square wave voltammetry (SWV) in a perchlorate buffer environment. We have also discussed that the morphology of the templated polymer is strongly influenced by the anionic content in the buffer according to the Hofmeister effect.[38,45] Therefore, as an extension to our prior work, the objective of this study is to validate the feasibility of using our proposed polymer-based neurochemical sensor platform in a physiologically relevant environment as well as of

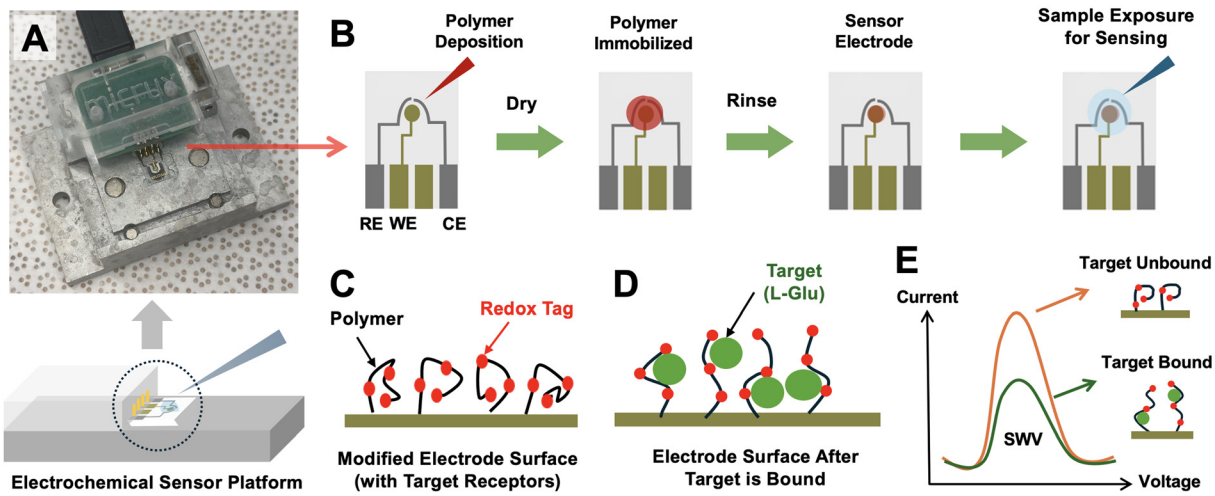

Fig. 1 The schematic overview of the electrochemical sensing strategy for L-glutamate detection using a redox-labeled polymer-modified electrode. (A) A commercial electrochemical sensing platform (MicruX Technologies) with a disposable electrode chip mounted on the connector; (B) the 3-electrode chip contains the reference (RE), the working (WE), and the counter (CE) electrodes. The sensor is prepared by polymer deposition onto the working electrode surface followed by subsequent drying and rinsing steps to remove excess polymers. The polymer-modified electrode is then exposed to the sample containing the target analyte for detection; (C) the polymer includes redox tags and undergoes conformational changes upon target (L-glutamate) binding, altering the spatial orientation of the redox labels relative to the electrode. In the absence of the target, the polymer remains folded, facilitating electron transfer; (D) in contrast, target binding induces polymer unfolding, resulting in a limited redox charge transfer and, therefore, a decrease in the peak current of square wave voltammetry (SWV); (E) this interaction can be quantitatively monitored *via* SWV where the changes in the peak current correlate with analyte concentration.

tracking the dynamic changes in the analyte concentration that may be occurring at the site of interrogation. To this end, this paper aims to investigate our polymer-based neurochemical sensor's capabilities of monitoring Glu in artificial cerebrospinal fluid (ACSF), a common buffer used in preparing *ex vivo* brain tissue samples, as well as in mice serum. Furthermore, we perform continuous monitoring of Glu and characterize the sensor's response to changes in Glu concentration in real-time.

2. Experimental section

2.1. Materials

N-Isopropylacrylamide (NIPAM, 97%), methacrylic acid (MAA, 99%), 4-vinylpyridine (VP, ≥95%), 2,2-azobis(isobutyronitrile) (AIBN, 98%), 2-(dodecylthiocarbonothioylthio)-2-methylpropanoic acid (DDMAT, 98%), *N*-methyl-L-glutamic acid (*N*-mGlu), L-glutamic acid (Glu, 99%), glycine (≥99%), γ-aminobutyric acid (GABA, ≥99%), aspartic acid (≥99%), 1,4-dioxane (anhydrous, 98%), sodium dithionite ($Na_2S_2O_4$, ≥99%), sodium hydroxide (NaOH, ≥98%), K_2OsCl_6 (99%, Alfa Aesar), 2,2′-bipyridine (bpy, 98%), ethyl ether (≥99%), ethylene glycol (anhydrous, 99.8%), *N*,*N*-dimethylformamide (DMF, 99.8%), 6-mercapto-1-hexanol ($C_6H_{14}OS$, >98.0%, TCI), sodium phosphate monobasic dihydrate (≥99%), magnesium chloride (≥98%), calcium chloride (≥97%), dextrose, and sodium bicarbonate ($NaHCO_3$, ≥99.7%) were purchased from Sigma-Aldrich and used without further purification. A thin-film double-metal (platinum for the reference and the counter electrodes and gold for the working electrode) single electrode from Micrux Technologies (Gijon, Spain) was used as a sensor chip for electrochemical measurements.

2.2. Instrumentation

The Bio-Logic VSP potentiostat (Seyssinet-Pariset, France) was employed to perform the cyclic voltammetry (CV) and the square wave voltammetry (SWV) for evaluating the sensor's performances. The Nicoya OpenSPR localized surface plasmon resonance (LSPR) benchtop system (Kitchener, ON, Canada) was used to analyze the polymer's binding affinity the target molecules. An Eppendorf 5910 centrifuge (Hamburg, Germany) was utilized for polymer purification and sample preparation. All working electrode potentials (voltages) are given with respect to the reference electrode (RE) of the chip.

2.3. Software

EC-Lab software (Bio-Logic, Seyssinet-Pariset, France) was used for all electrochemical measurements, and OriginPro (OriginLab Corporation, Northampton, MA, USA) was utilized for post-processing, including plotting electrochemical data, performing curve fitting, and statistical analysis. TraceDrawer (Ridgeview Instruments, Uppsala, Sweden) was used for analyzing the SPR sensorgram's real-time responses, curve-fitting the measured data, and extracting the parameters for the polymer's binding kinetics.

2.4. Preparation of artificial cerebrospinal fluid (ACSF)

NaCl (3.65 g), KCl (0.112 g), NaH_2PO_4 (0.085 g), $MgCl_2$ (0.0475 g), $CaCl_2$ (0.11 g), and dextrose (0.36 g) were added to 450 mL of DI water, and the mixture was stirred for about 10 minutes until fully dissolved. Separately, $NaHCO_3$ (1.09 g) was measured and dissolved in 50 mL of DI water to ensure complete dissolution. Prior to experimental use, the two solutions were mixed and stirred thoroughly. Finally, the solution was purged with carbogen ($5\%CO_2/95\%O_2$) to stabilize the pH to about 7.4 and the mixture was stirred for 30 minutes.

2.5. Synthesis of poly (NIPAM-VP-MAA) copolymer

The polymer was prepared in the same manner as described previously.[38] Briefly, in a three-neck round-bottom flask, NIPAM (3.2 g), MAA (0.32 mL), VP (0.56 mL), DDMAT (0.136 g), *N*-mGlu (0.064 g), and AIBN initiator (0.03 g) were added to 25 mL of dioxane. All openings in the flask, except for the condenser, were sealed with Parafilm. Nitrogen was flown into the flask for 5 minutes to remove all oxygen. Afterward, the flask was completely sealed and was submerged in the oil bath. The bath temperature was ramped up to 80 °C to initiate the RAFT polymerization for 24 hours. Once the reaction is complete, the flask was cooled to room temperature, and the mixture was purified using diethyl ether, a non-solvent, three times. A centrifuge was used to separate the polymer from the non-solvent. Purification was repeated until the solution became clear. The purified polymer was then dehydrated under a hood and transferred to a 50 °C oven for drying, completing the polymer synthesis. The polymer powder was dissolved in DI water and transferred into a dialysis tube with a MWCO of 1 kDa. The tube was immersed in DI water for three days, with the bath water changed every four hours. To remove excess water from the polymer, it was stirred at 50 °C and then placed in a vacuum oven at 40 °C for a day. It should be noted that, although our sensor's target analyte is L-Glutamate (L-Glu), *N*-mGlu was used as a substitute template during our polymer synthesis. The reason for this substitution is because L-Glu has poor solubility in dioxane and using it as a template resulted in a low yield of the synthesized polymers. However, due to the similarities in the molecular structure between the two, our polymers templated with *N*-mGlu have shown high selectivity toward both *N*-mGlu as well as L-Glu.[38]

2.6. Synthesis of $Os(bpy)_2Cl_2$ complex

Following the previously described protocol,[38] the $Os(bpy)_2Cl_2$ complex was synthesized. Briefly, K_2OsCl_6 (150 mg) and 2,2′-bipyridine (97 mg) were dissolved in 10 mL of DMF and agitated for three hours at 140 °C. For removing the KCl crystals developed during the cooling step, a paper filtration method was used. The $Os(bpy)Cl_3{\cdot}H_2O$ complex powder was precipitated by adding 40 mL of ethyl ether and 5 mL of ethanol to the residual solution. Centrifugation was used to gather the Os

(bpy)Cl_3·H_2O powder, which was then left to dry overnight. A solution of H_2O/DMF/methanol (20 mL : 2 mL : 1 mL) was used to dissolve this powder. This solution was mixed with a saturated $Na_2S_2O_4$ to precipitate and produce the powdered Os(bpy)$_2Cl_2$ complex. The Os(bpy)$_2Cl_2$ powder was then dried for 48 hours at 50 °C in a vacuum oven.

2.7. Synthesis of osmium-grafted copolymer poly (NIPAM-VP-MAA)-*g*-Os(bpy)$_2$Cl

Poly (NIPAM-VP-MAA)-*g*-Os(bpy)$_2$Cl was made according to the procedure described previously.[38] The synthesized poly (NIPAM-VP-MAA) copolymer (300 mg) and the Os(bpy)$_2Cl_2$ complex (180 mg) were dissolved in 5 mL of ethylene glycol and purged with N_2 gas for about 5 minutes, then stirred at 140 °C for 24 hours. After cooling down the solution, it was poured into a dialysis tube with a 1 kDa molecular weight cut-off (MWCO) to remove the remaining Os(bpy)$_2Cl_2$. The dialysis tubing was inserted into DI water for 3 days, with the water bath being changed every 4 hours. The polymer solution was stirred at 40 °C to remove water followed by placing it in a vacuum oven at 40 °C for 24 hours to obtain a fully dried osmium-grafted polymer powder.

2.8. Preparation of the sensor electrode and electrochemical measurements

The gold working electrode was cleaned by dropping DMF on the surface of the sensors and was allowed to sit for about 30 minutes. Then the surface of the electrode was thoroughly washed using DI water and blow dried with an air gun. 1 mg of poly (NIPAM-VP-MAA)-*g*-Os(bpy)$_2$Cl and 1 mg of DTT (Dithiothreitol) were dissolved in 30 μL DMF and stirred for about 90 minutes. Afterward, 5 μL of the MCH was added to the polymer solution and stirred for 15 minutes. Then, 5 μL of the prepared solution was dropped on the working electrode of the chip and dried overnight. Prior to the experiment, at least 15 runs of cyclic voltammetry (CV) were performed (with each run consisting of 10 cycles) to ensure that a stable CV curve was obtained. The CV analysis was performed in the potential range of −0.5 V to +0.5 V *vs.* RE with a scan rate of 100 mV s^{-1} in ACSF solution for all experiments unless mentioned otherwise. This step was repeated until stable current measurements were achieved.

After achieving equilibrium, square wave voltammetry (SWV) was performed in the potential range of −0.6 V to +0.6 V *vs.* RE with a pulse height of 10 mV, a pulse width of 100 ms, and a step height of 10 mV. The process was repeated until a stable peak current was consistently obtained. For L-Glu detection experiments, ACSF solutions containing a known concentration of L-Glu in the range of 1 nM–1 μM were each prepared through serial dilution. Then, 20 μL of the prepared sample L-Glu solution was dropped on the surface of the sensor chip, and the results were recorded using EC-Lab. For each SWV measurement, the peak current (*i.e.*, ΔI) value was obtained after performing the background subtraction on OriginPro software. A fresh electrolyte solution was used for each experiment.

2.9. Sample preparation for the SPR analysis

For the SPR experiments, the target molecules (*N*-mGlu) were immobilized onto the SPR sensor chip while flowing the solution containing the polymers over the surface of the chip to allow the interaction between the polymer and the analyte. Since the polymers have a higher molecular weight (~8 kDa) than the target molecules (~0.16 kDa), the polymer binding to the *N*-mGlu molecule anchored on the chip caused a significant increase in the SPR's sensorgram response. To immobilize the ligand molecules (*N*-mGlu) to the SPR chip, the amine-functionalized SPR sensor chip, provided by the instrument's manufacturer, was used according to the company's user manual. The polymer solution was prepared by dissolving poly (NIPAM–VP-MAA) polymer (1.2 mg) in 10 mL of ACSF to achieve a concentration of 20 μM as a stock solution, followed by continuous stirring for 24 hours. ACSF was also used as the running buffer during the SPR measurements.

Initially, the running buffer was injected into the SPR system at the maximum flow speed of 150 μL min^{-1}. The bubble removal step was completed by injecting 80% isopropanol. The ligand solution was prepared by dissolving 4.5 mg of EDC, 2.7 mg of NHS, and 20 mg of *N*-mGlu into 350 μL of the activation buffer (provided by Nicoya Lifesciences) and incubating the mixture for 1 hour. This allows the carboxyl groups of the *N*-mGlu to be coupled to the chip's amine groups. Once the ligand solution is activated, the flow rate was then reduced to 20 μL min^{-1}, and the ligand was injected into the instrument. Afterward, a blocking solution (provided by Nicoya Lifesciences) was introduced, followed by a regeneration buffer (100 mM NaOH) with a flow rate of 100 μL s^{-1}. To measure the interaction between the polymers and the ligands, the polymer solution was introduced to the SPR chip with a flow rate of 20 μL s^{-1}. After each analyte injection, the regeneration buffer was injected to remove the bound polymers.

3. Results and discussion

3.1. Polymer characterization

To confirm the polymer's molecular composition, NMR and FTIR were performed. The NMR analysis (Fig. S1 in SI) resulted in the molar ratio of the NIPAM, VP, and MAA is 71.3%, 10.6%, and 18.1%, respectively, indicating that the polymers were synthesized as designed and are consistent with our previous reporting.[38] The FTIR analysis (Fig. S2 in SI) also verified the successful synthesis of poly (NIPAM-VP-MAA), Os(bpy)$_2Cl_2$, and the grafting of Os(bpy)$_2Cl_2$ onto the polymer backbone to yield poly (NIPAM-VP-MAA)-*g*-Os(bpy)$_2$Cl.[37,38] Furthermore, the polymer's average molecular weight (MW = 6.258 kDa) and the polydispersity index (PDI = 1.49) obtained by gel permeation chromatography (GPC) as well as the surface chemistry analysis of immobilizing the polymers on the gold electrode using X-ray photoelectron spectroscopy (XPS) have been extensively studied in our previous work.[37,38]

Based on the polymer's average molecular weight, each polymer is expected to have on average 1–2 target binding

sites. However, adjusting the length of the polymer chain can significantly influence the polymer's sensing performances. For example, as the polymer becomes longer, the sensor response will become more sensitive due to a greater change in the conformation and therefore the greater displacement of the redox-active labels. However, the sensor's response time may increase due to the potential interchain interactions and the 'tangling' of the polymers which may delay the target-induced conformation change. Conversely, as the polymer becomes shorter, a faster response may be expected due to reduced interchain interaction and the target's easy access to the binding sites. However, the sensitivity may be reduced due to the polymer's shorter actuation distance.

Our previous XPS analysis suggests that the polymer immobilization on gold electrode using reducing agents such as TCEP and DTT to form thiol bonding leads to mostly chemisorbed and covalently bound polymers.[37] Also, RAFT polymers can be easily attached to gold electrodes *via* thiol chemistry because the RAFT chain transfer agent (DDMAT), which is the crosslinking molecule between the polymer and the electrode, contains three sulfur atoms (trithiocarbonate). Upon its reduction, multiple Au–S covalent bonds can be formed between the RAFT agent of the polymer and the gold surface resulting in a high yield of chemisorbed polymers. The SEM imaging of the working electrode surface (Fig. S3 in SI) further confirms the successful immobilization of the polymer-based glutamate-binding receptors on the electrochemical sensor.

Although the synthesis procedure of the polymer may appear to be complex and time consuming at first, the protocol is actually quite straight forward and can be batch processed in large scale. Also, the majority of the synthesis time is spent on purifying the polymers using dialysis which could take a few days. One of the benefits of using RAFT polymerization technique is that it is a highly controlled and reproducible process resulting in high yield of polymerization with uniform molecular weight distribution. In summary, the polymer synthesis procedure can be streamlined into a simplified batch process with minimum human labor to produce polymers with high yield and low cost.

3.2. Characterization of the templated polymer's binding affinity to glutamate in ACSF buffer

To verify the synthesized polymer's affinity to the template molecule *N*-mGlu (which has a similar molecular structure to our target analyte L-Glu), the real-time Surface Plasmon Resonance (SPR) measurement was performed on the polymer against *N*-mGlu. In the SPR analysis, the osmium complexes were not incorporated into the polymers because they do not actively participate in the target binding mechanism, and furthermore, the presence of these redox-active molecules could potentially interfere with the SPR sensorgram measurements. Our previous work has reported that the inclusion of the osmium-based redox tags can negatively impact the target affinity of the polymers,[38] and therefore, to achieve the desired sensing performances (*e.g.*, target selectivity and sensitivity), optimizing the molar ratio of the osmium complex in the polymer may be required. The SPR sensorgram's concentration dependent response indicates that specific bidning between the templated polymers and *N*-mGlu molecules are occurring as shown in the binding phase in Fig. 2A. Furthermore, upon injecting the running buffer (ACSF) to the sensor chip, the dissociation between the templated polymers and the target can be observed in the unbinding phase. This suggests that the binding kinetics between the templated polymers and *N*-mGlu is highly specific and reversible where the association and dissociation is occurring simultaneously to establish an equilibrium binding constant (K_D). To validate the effectiveness of molecular templating during the polymer synthesis step, the SPR sensorgram for the non-templated polymers, which were synthesized in the absence of the template, is also shown (Fig. 2B) where a significantly reduced responses to *N*-mGlu injection is observed compared to the templated polymer's case. Based on the curve-fitted Hill–Langmuir model of our real-time SPR data, the equilibrium binding constants of K_D = 0.95 μM and K_D = 5.85 μM were obtained (Fig. 2C) for the templated and non-templated polymers, respectively, indicating that the templating process significantly enhances the polymer's affinity to *N*-mGlu molecules.

3.3. Electrochemical detection of glutamate in ACSF buffer

To implement the electrochemical Glu sensor, the templated polymers are first immobilized on the gold working electrode by drop casting the polymer solution following the protocol described in the previous section. The concentration of the polymer solution was optimized to be 400 μM based on our prior studies.[38] Once the sensor electrode is prepared, square-wave voltammetry (SWV) was performed on the electrode after exposing it to Glu. Fig. 3A shows that, as the exposed Glu concentration increases, the voltammetry current peak decreases suggesting that, upon target binding, the polymer conformation changes from a folded to an unfolded configuration. This results in a decrease in the SWV peak current, namely a "signal-off response", because the redox labels (*i.e.*, the osmium molecules) in the polymers have moved away from the electrode due to the unfolding of the polymers (Fig. 1E). Furthermore, unlike the SWV curves of the templated polymer-based sensor which show a Glu concentration-dependent voltammetry signal change, the non-templated polymer showed minimal Glu-dependent SWV responses as evidenced by the similar peak heights for all Glu concentrations tested. The calibration curves (SWV peak values) in Fig. 3B show that the developed biosensor is able to detect Glu in the concentration range of 10 nM–500 nM while the electrode immobilized with non-templated polymers showed no significant differences in the response for the same concentration range. To characterize the sensor's target selectivity, the templated polymer-based Glu sensor was exposed to various neurochemicals that could potentially interfere with Glu detection, and the peak SWV currents were observed. As can be seen in Fig. 3C, our sensor is most responsive to Glu while it also shows moderate levels of responses to other chemicals tested. These non-specific sensor responses to other neurochemicals can be attributed to the

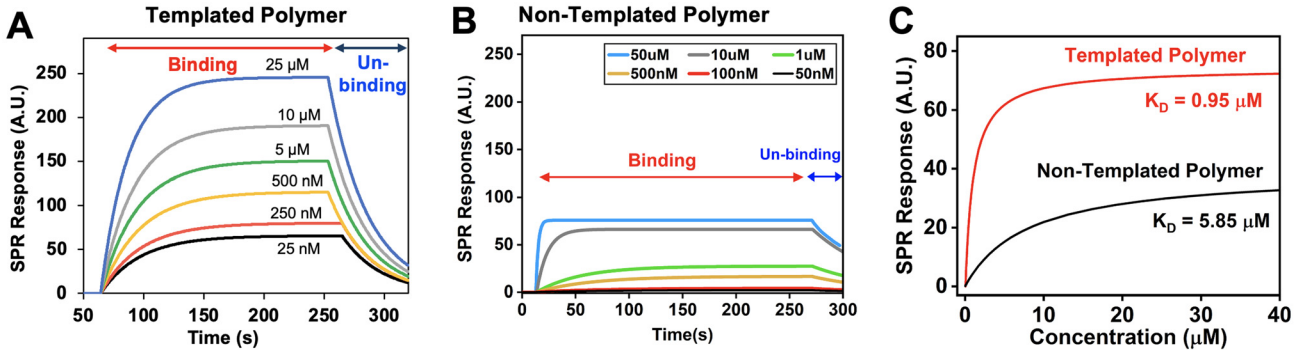

Fig. 2 Surface Plasmon Resonance (SPR) analyses of the polymer-based Glu receptors in ACSF buffer. (A) Real-time SPR sensorgram responses for the templated polymers; and (B) the non-templated polymers when interacting with *N*-mGlu; and (C) the corresponding Hill–Langmuir binding affinity curves for both polymers.

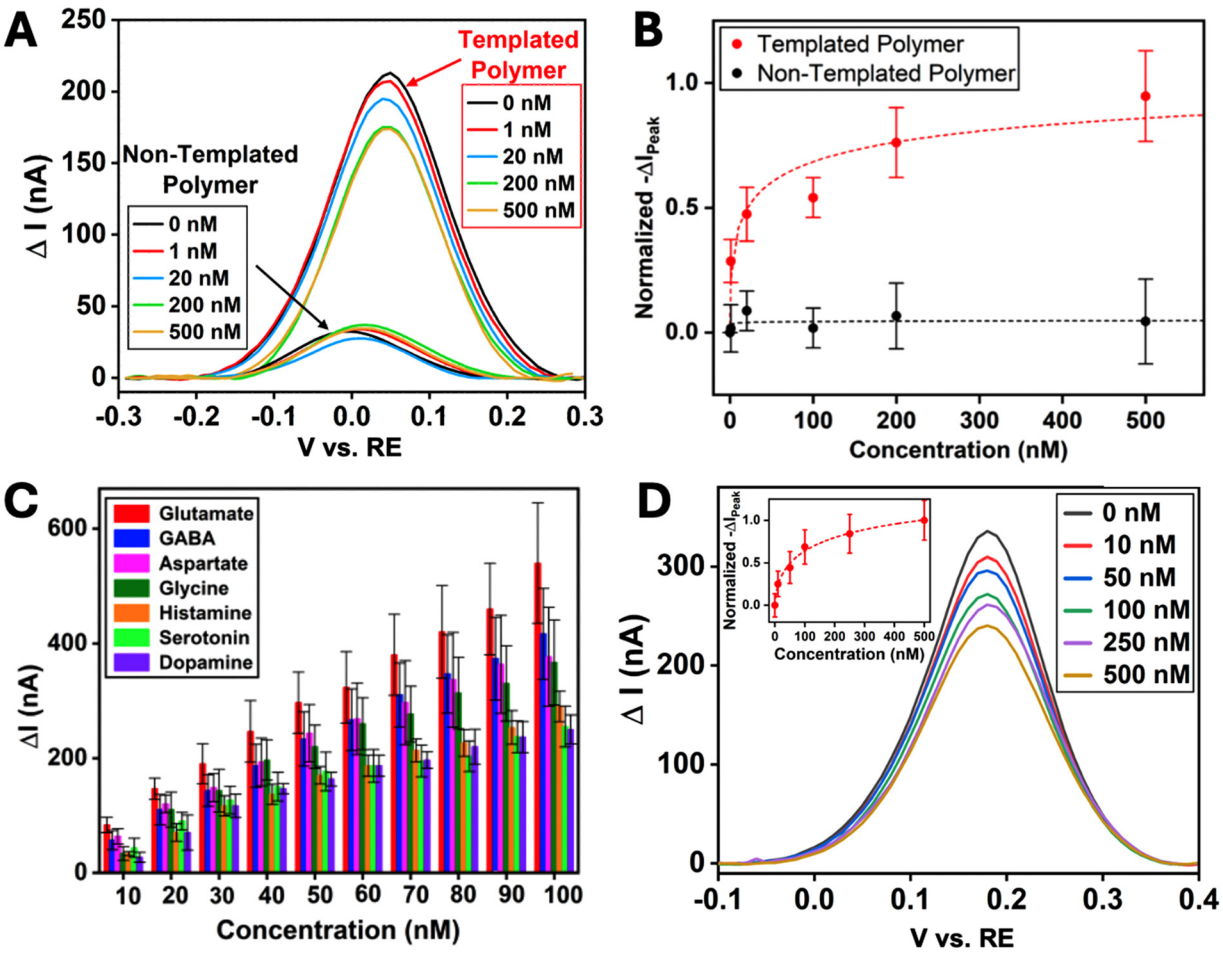

Fig. 3 Electrochemical sensing of glutamate (Glu) using the polymer-based sensor platform. (A) Square-wave voltammetry (SWV) curves of the templated *vs.* non-templated polymer-immobilized electrodes after exposure to various concentrations of Glu in 1X ACSF buffer; (B) the calibration curves (SWV peak current) for the templated *vs.* non-templated polymer-based Glu biosensors in ACSF. Error bar is 1 standard deviation (n = 4); (C) chemical selectivity characterization of the templated polymer-based Glu biosensor against potential interfering species. Error bar is 1 standard deviation (n = 3); and (D) SWV curves of the Glu biosensor response in mice serum spiked with various concentrations of Glu. The inset shows the sensor's calibration curve in mice serum. Error bar is 1 standard deviation (n = 3).

similarities in the molecular structures between the target and the other molecules tested. The main interfering species to Glu is gamma-aminobutyric acid (GABA), the primary inhibitory neurotransmitter in the brain that often works to modulate or suppress the excitatory functions of Glu.[46] One possible approach to minimize the interference and/or false-positive

sensor responses from non-target species during Glu measurements in tissue samples is to employ various pharmacological techniques such as introducing receptor blockers to temporarily reduce or suppress the release of unwanted interfering chemicals.

For further validation of the proposed glutamate sensor in real physiological samples, the templated polymer-based sensor was tested using mice serum (Sigma-Aldrich) spiked with various concentrations of Glu. As shown in Fig. 3D, a concentration-dependent "signal-off" behavior similar to that observed in ACSF (Fig. 3A) was obtained in mice serum samples. The corresponding calibration curve (inset in Fig. 3D) further demonstrates the capability of the developed sensor platform to detect glutamate in real biological samples within the 10–500 nM range, indicative of its practicality. The SWV response suggests that the polymer layer maintains a similar morphological state in mice serum as in the ACSF environment with the ability to undergo phase transition between folded and unfolded configurations. In addition, it is worth noting that the SWV curves in mice serum were more stable and consistent than when tested in ACSF. This improved stability of our Glu sensor in mice serum can be attributed to the serum's excellent buffering capability in maintaining the pH of the fluid compared to that of ACSF where the pH could possibly drift as the oxygen content gradually changes over time. Indeed, the pH of the serum sample was measured to be 7.6 throughout the duration of the experiment with no noticeable changes even after spiking with glutamate.

Due to the inherent pH responsiveness of the polymer (poly NIPAM) used in our glutamate receptor, the sensor may exhibit sensitivity to local pH changes. However, this regional pH sensitivity of the polymer can be beneficial for promoting selectivity of the sensor because other structurally similar species will protonate or deprotonate differently than glutamate resulting in poor binding to the polymer. It should be noted that, while regional pH changes near the polymer can assist in improving target selectivity, overall pH changes in the whole sample fluid can adversely impact our sensor's performance, and therefore it is critical to maintain the overall pH of the sample solution to a constant value. Fortunately, oxygenated ACSF, which is often used for measurements in sectioned brain slices, has the buffering capability to main its pH to a constant level. Also, the overall pH levels in the extracellular area of *in vivo* models are not expected to change dramatically. Therefore, the pH responsiveness of our polymer-based receptor should not be a major concern for its use in biological models.

In our previous work, we demonstrated that our polymer-based biosensors exhibited a "signal-on" response in perchlorate ($NaClO_4$) buffer where the SWV peak current increased as the glutamate concentration increased. This suggests that the polymer is normally in an unfolded conformation but transitions to a folded shape upon target binding when ClO_4^- ions are present. However, in the ACSF environment, the polymer exhibits the opposite behavior (*i.e.*, "signal-off") indicating that the polymers are normally in a folded morphology due to the type of anions present in ACSF. The Hofmeister effect suggests that kosmotropic ions tend to cause our polymer to collapse into a globular form while chaotropic ions tend to open up the polymer into an untangled form.[45,47,48] Since ACSF is kosmotropic while perchlorate buffer is chaotropic, our polymer-based sensor's detection mechanism, whether signal-on or -off, depends on the type of buffer used during the measurement.

3.4. Frequency dependence on the electrochemical signaling of the polymer-based receptors

In addition to the influences by the anions in the buffer, the templated polymer's signaling mechanism (*i.e.*, signal-on or -off) is also affected by the frequency of the SWV. For example, the signaling mechanism at high frequencies may be inverted (from signal-on to -off and *vice versa*) compared to that at low frequencies.[49] The kinetic differential measurement (KDM) is a well-known technique for aptamer-based electrochemical sensors that takes advantage of this phenomenon and measures SWV at two different frequencies to eliminate the drift in the signal that is common at both frequencies.[41] To characterize the frequency dependent signaling behavior of our polymer receptors, the SWV of the Glu sensor was conducted under different frequencies ranging from 1 Hz to 100 Hz. As shown in Fig. 4, the signaling behavior of the templated Glu-binding polymer is "signal-on" at low frequencies (mostly between 1–5 Hz) and "signal-off" at high frequencies (10–100 Hz). To achieve both reasonably fast sampling time as well as sensitive Glu detection, we chose 5 Hz as a frequency for all SWV measurements in this work (for both static and continuous measurements).

3.5. Continuous real-time monitoring of glutamate in ACSF

To evaluate our biosensor's ability to monitor Glu continuously in real-time, the SWV was applied repeatedly, and the peak current value was tracked for each SWV cycle. The same SWV parameters used in the static Glu measurements were used in the continuous monitoring experiments. While SWV was running repeatedly, droplets of ACSF solution with increasing concentrations of Glu (0, 1, 20, 100, 200, 500 nM, and 1 μM) were sequentially placed on the working electrode of the sensor with each sample droplet having a volume of 20 μL. At least 10 seconds were allowed between each addition of the sample droplet to ensure that equilibrium in Glu concentration is reached.

Upon a step change in the Glu concentration, the sensor's readout responded immediately as indicated by the sudden change in the peak current value of the SWV. However, reaching a stable response took substantially longer on the order of 1 minute (Fig. 5A). One possible reason for such prolonged stabilization time is that the polymer may be undergoing adjustments in the morphology due to the changing ionic environment caused by the instant Glu concentration change. Also, there may be interchain interactions among neighboring polymers due to the overcrowding of the polymers on the electrode surface. We expect that further miniaturization of the

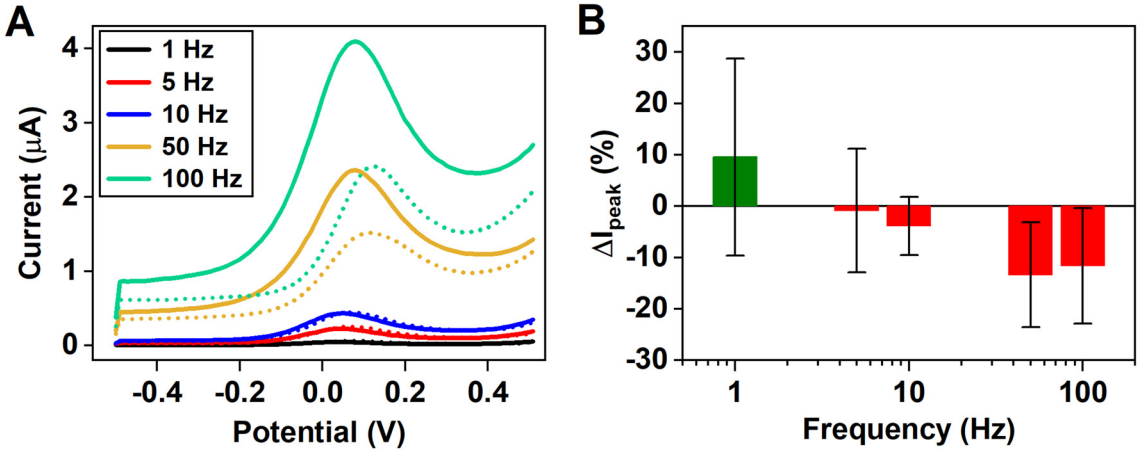

Fig. 4 The frequency-dependent kinetic response of the polymer-based Glu sensor. (A) SWV responses at various frequencies (1 Hz–100 Hz) before (dashed lines) and after (solid lines) exposure to 1 μM of Glu in ACSF; (B) plot of ΔI_{peak} (peak SWV current after Glu binding – peak SWV current before Glu binding) as a function of the frequency. Error bar = 1 standard deviation (n = 4).

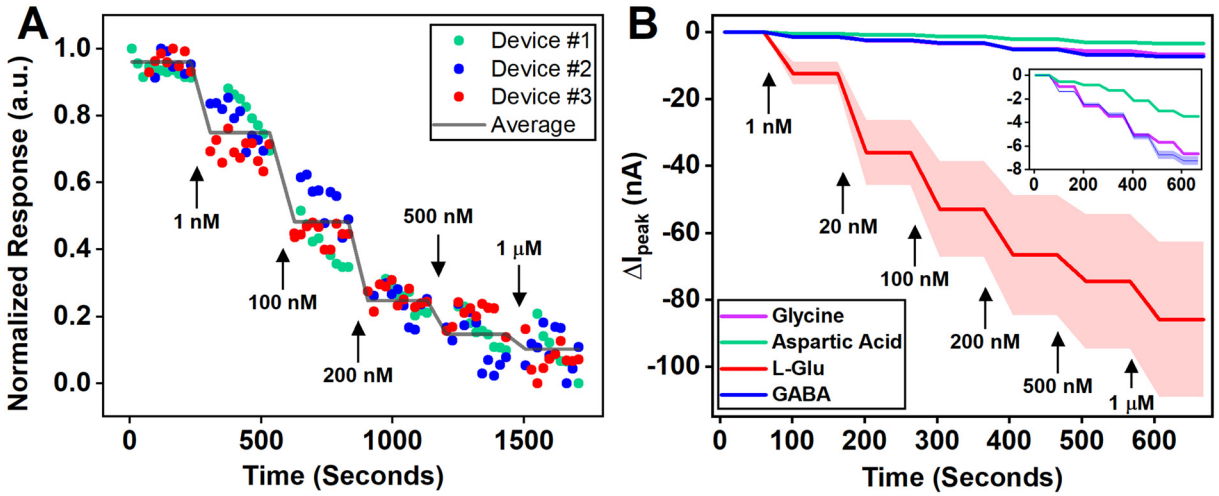

Fig. 5 Continuous real-time monitoring of Glu using the templated polymer-based sensor. (A) Normalized responses (peak SWV current) as a function of time during sequential step changes in the Glu concentration (0, 1, 100, 200, 500 nM, and 1 μM). The line indicates the average value of 10 consecutive SWV peak current values for each concentration; (B) continuous responses of the polymer-based biosensor when exposed to glycine, aspartic acid, Glu, and GABA. The line indicates the average value of the SWV peak current for each concentration. The shaded region represents 1 standard deviation (n = 3). The inset is the magnified plot for glycine, aspartic acid, and GABA.

electrode into microscale and precise controlling of the polymer surface coverage (both density and uniformity) will significantly improve the response time and stability of this early-stage exploratory sensor platform. While it is important to acknowledge that enzymatic electrochemical sensors are able to achieve much faster response times (on the order of seconds), the target-templated polymer-based sensor offers features that complement some of the challenges that exist with enzymatic sensors such as limited lifetime, stability issues to changing enzymatic activities, and device miniaturization.

The selectivity of the real-time glutamate sensor was also evaluated by operating our sensor under continuously repeating SWV measurements under 3 other neurochemicals, glycine, aspartic acid, and γ-aminobutyric acid (GABA), that may act as potential interfering species. Each of these non-target chemicals was prepared in ACSF and tested under the same conditions used for the Glu detection. The current changes observed upon introducing glycine and aspartic acid were negligible, indicating that these molecules did not interact significantly with the templated polymer receptor (Fig. 5B). A minor response was observed with GABA; however, the magnitude of this response was substantially lower than that elicited by glutamate, even at equivalent concentrations. A notable concern for the real-time measurement is the inherent variability of the sensor's response to Glu as indicated by the

Table 1 Comparison of the spatiotemporal resolutions of established glutamate sensing techniques

Technique	Temporal resolution	Spatial resolution	Pros	Cons
Patch clamp[21,23,50,51]	<1 millisecond	~1 μm	High spatiotemporal resolution	Lack of chemical selectivity, limited spatial mapping
Microdialysis[52–55]	5–15 minutes	~250 μm	Compatible with awake and freely moving animals, simultaneous multi-analyte sampling	Low spatiotemporal resolution, limited spatial mapping
Enzymatic electrochemical sensor[30,35,56]	2–10 seconds	~30 μm	Good spatiotemporal resolution	Enzyme stability issues, signal drift
Genetically encoded sensor (iGluSnFR)[24,25,57–60]	~20 milliseconds	~200 nm	High spatiotemporal resolution, large field of view	Lack of quantitative measurements, complex genetic modification of the target cells

shaded area in (Fig. 5B). This can be attributed to, among other factors, the inability to calibrate the sensor during the continuous real-time mode. We also believe that, as mentioned above, miniaturization and polymer density control would further enhance the reproducibility of the real-time monitoring. Furthermore, as a future direction, incorporating an advanced machine learning algorithm into our sensing methodology may be the next logical step to improving our sensor's reliability and accuracy and to bring this technology closer to *in vivo* measurements in physiological models.

Table 1 summarizes the spatial and temporal resolutions of the conventional techniques for measuring glutamate. Since our polymer-based Glu sensor is in its early exploratory stage, its resolution is not quite comparable to the techniques presented in the table. However, due to the sensor's simple design and architecture, the proposed sensor platform has the potential to achieve significantly improved spatiotemporal resolution through device miniaturization and finetuning of our polymer-based receptors.

4. Conclusion

A new stimuli-responsive, polymer-based biosensor was developed for the non-enzymatic measurement of the neurotransmitter glutamate (Glu). The templated polymer employed was poly (NIPAM-VP-MAA)-*g*-Os(bpy)$_2$Cl. This polymer was synthesized using the RAFT polymerization method, and an osmium complex was grafted onto it to serve as a redox tag. It was observed that in ACSF, a moderately kosmotropic solution, the polymer exhibited a signal-off response upon interaction with the target molecule. The electrochemical measurements suggest that, in the absence of the target, the polymer remained folded and closed, while specific target recognition caused the polymer to unfold and expand. Minimal responses were observed when the sensor was exposed to other interfering neurotransmitters including GABA, aspartic acid, and glycine, demonstrating the polymer's high selectivity toward Glu. Both static (fixed Glu concentration) and dynamic (Glu concentration changing in real-time) measurements were explored, and the biosensor was able to track the step changes in Glu concentration with reasonably rapid response time, highlighting its potential suitability for continuous real-time monitoring applications. The sensor also exhibited reliable Glu measurement in mice serum with the detection range of 10–500 nM demonstrating its utility in real physiological samples. Additionally, SPR results revealed that the templated polymer exhibited a higher affinity toward the target compared to the non-templated version of the polymer indicating that the templating process improves target selectivity. In conclusion, this work demonstrated the proposed biosensor's feasibility to be used in monitoring Glu in physiologically relevant environments and conditions. For measurements in biological samples such as tissue slices, this technology could be further expanded into the development of a wire-like implantable probe modified with our polymer-based receptors for the direct monitoring of Glu from the tissue.

Author contributions

LAA, AA, and ES conceived the research and designed the experiments. LAA, SM, and MB carried out the experiments. SM and ES wrote the original draft of the article. All authors contributed to the analyses of the data and editing of the article.

Conflicts of interest

There are no conflicts to declare.

Data availability

The data supporting this paper have been included in the main article and in the supplementary information (SI). The supplementary information includes: (1) NMR Analysis; (2) FT-IR Analysis; and (3) SEM Imaging of the polymer-based glutamate receptors. See DOI: https://doi.org/10.1039/d5an01088h.

Acknowledgements

The authors gratefully acknowledge Patricia Stone from the University Instrumentation Center (UIC) at the University of

New Hampshire (UNH) for her assistance with NMR and FTIR analyses. The use of Surface Plasmon Resonance (SPR) was supported by the UNH Center for Integrated Biomedical and Bioengineering Research (CIBBR), through funding from the National Institute of General Medical Sciences (NIGMS). This research was funded by the National Institute of Biomedical Imaging and Bioengineering (NIBIB, Award 1R21EB031433), the National Science Foundation (NSF, Award 1847152), the National Institute of General Medical Sciences (NIGMS, Award P20GM113131), and the National Institute of Mental Health (NIMH, Award R01MH124811).

References

1 A. Citri and R. C. Malenka, Synaptic Plasticity: Multiple Forms, Functions, and Mechanisms, *Neuropsychopharmacology*, 2008, **33**(1), 18–41, DOI: 10.1038/sj.npp.1301559.
2 S. S. Willard and S. Koochekpour, Glutamate, Glutamate Receptors, and Downstream Signaling Pathways, *Int. J. Biol. Sci.*, 2013, **9**(9), 948–959, DOI: 10.7150/ijbs.6426.
3 J. V. Andersen, The Glutamate/GABA-Glutamine Cycle: Insights, Updates, and Advances, *J. Neurochem.*, 2025, **169**(3), e70029, DOI: 10.1111/jnc.70029.
4 I. Varvari, L. Bolte, C. Colli, V. Mancini, M. M. Nour, P. McGuire and R. A. McCutcheon, Glutamatergic Modulation of Brain Function in Psychosis: A Systematic Review of Neuroimaging Studies, *Biol. Psychiatry Cogn. Neurosci. Neuroimaging*, 2025, **10**(12), 1221–1238, DOI: 10.1016/j.bpsc.2025.07.004.
5 L. Song, J. Dong, W. Cheng, Z. Fei, R. Wang, Z. He, J. Pan, L. Zhao, H. Wang and R. Peng, The Role of Glutamatergic Neurons in Changes of Synaptic Plasticity Induced by THz Waves, *Biomolecules*, 2025, **15**(4), 532, DOI: 10.3390/biom15040532.
6 R. Celli, I. Santolini, G. Van Luijtelaar, R. T. Ngomba, V. Bruno and F. Nicoletti, Targeting Metabotropic Glutamate Receptors in the Treatment of Epilepsy: Rationale and Current Status, *Expert Opin. Ther. Targets*, 2019, **23**(4), 341–351, DOI: 10.1080/14728222.2019.1586885.
7 B. F. Gruenbaum, A. Schonwald, M. Boyko and A. Zlotnik, The Role of Glutamate and Blood–Brain Barrier Disruption as a Mechanistic Link between Epilepsy and Depression, *Cells*, 2024, **13**(14), 1228, DOI: 10.3390/cells13141228.
8 R. Wang and P. H. Reddy, Role of Glutamate and NMDA Receptors in Alzheimer's Disease, *J. Alzheimer's Dis.*, 2017, **57**(4), 1041–1048, DOI: 10.3233/JAD-160763.
9 Y. Gong, C. F. Lippa, J. Zhu, Q. Lin and A. L. Rosso, Disruption of Glutamate Receptors at Shank-Postsynaptic Platform in Alzheimer's Disease, *Brain Res.*, 2009, **1292**, 191–198, DOI: 10.1016/j.brainres.2009.07.056.
10 N. Fayed, P. J. Modrego, G. Rojas-Salinas and K. Aguilar, Brain Glutamate Levels Are Decreased in Alzheimer's Disease: A Magnetic Resonance Spectroscopy Study, *Am. J. Alzheimers Dis. Other Demen.*, 2011, **26**(6), 450–456, DOI: 10.1177/1533317511421780.
11 C. Soares, L. U. Da Ros, L. S. Machado, A. Rocha, G. Lazzarotto, G. Carello-Collar, M. A. De Bastiani, J. P. Ferrari-Souza, F. Z. Lussier, D. O. Souza, P. Rosa-Neto, T. A. Pascoal, B. Bellaver and E. R. Zimmer, The Glutamatergic System in Alzheimer's Disease: A Systematic Review with Meta-Analysis, *Mol. Psychiatry*, 2024, **29**(7), 2261–2273, DOI: 10.1038/s41380-024-02473-0.
12 Z. Zhang, S. Zhang, P. Fu, Z. Zhang, K. Lin, J. K.-S. Ko and K. K.-L. Yung, Roles of Glutamate Receptors in Parkinson's Disease, *Int. J. Mol. Sci.*, 2019, **20**(18), 4391, DOI: 10.3390/ijms20184391.
13 N. H. Almohmadi, H. M. Al-kuraishy, A. I. Al-Gareeb, A. K. Albuhadily, A. M. Abdelaziz, M. S. Jabir, A. Alexiou, M. Papadakis and G. E.-S. Batiha, Glutamatergic Dysfunction in Neurodegenerative Diseases Focusing on Parkinson's Disease: Role of Glutamate Modulators, *Brain Res. Bull.*, 2025, **225**, 111349, DOI: 10.1016/j.brainresbull.2025.111349.
14 A. Marsman, M. P. van den Heuvel, D. W. J. Klomp, R. S. Kahn, P. R. Luijten and H. E. Hulshoff Pol, Glutamate in Schizophrenia: A Focused Review and Meta-Analysis of ^{1}H-MRS Studies, *Schizophr. Bull.*, 2013, **39**(1), 120–129, DOI: 10.1093/schbul/sbr069.
15 D. Boison, P. Singer, H.-Y. Shen, J. Feldon and B. K. Yee, Adenosine Hypothesis of Schizophrenia–Opportunities for Pharmacotherapy, *Neuropharmacology*, 2012, **62**(3), 1527–1543, DOI: 10.1016/j.neuropharm.2011.01.048.
16 J. T. Coyle, Passing the Torch: The Ascendance of the Glutamatergic Synapse in the Pathophysiology of Schizophrenia, *Biochem. Pharmacol.*, 2024, **228**, 116376, DOI: 10.1016/j.bcp.2024.116376.
17 A. S. Guzman, M. P. Avalos, L. N. De Giovanni, P. V. Euliarte, M. A. Sanchez, B. Mongi-Bragato, D. Rigoni, F. A. Bollati, M. B. Virgolini and L. M. Cancela, CB1R Activation in Nucleus Accumbens Core Promotes Stress-Induced Reinstatement of Cocaine Seeking by Elevating Extracellular Glutamate in a Drug-Paired Context, *Sci. Rep.*, 2021, **11**(1), 12964, DOI: 10.1038/s41598-021-92389-4.
18 M. Abdullah, S.-H. Lin, L.-C. Huang, M. I. Khan, C.-C. Kung and Y. K. Yang, Cue-Induced Magnetic Resonance Spectroscopy of Glutamate in Addiction Research: Current Evidence, Pros, and Cons, *Clin. Psychopharmacol. Neurosci.*, 2025, **23**(3), 327–336, DOI: 10.9758/cpn.24.1254.
19 T. D. Prickett and Y. Samuels, Molecular Pathways: Dysregulated Glutamatergic Signaling Pathways in Cancer, *Clin. Cancer Res.*, 2012, **18**(16), 4240–4246, DOI: 10.1158/1078-0432.CCR-11-1217.
20 M. T. P. De Aquino, T. W. Hodo, S. G. Ochoa, R. V. Uzhachenko, M. A. Mohammed, J. S. Goodwin, T. Kanagasabai, A. V. Ivanova and A. Shanker, Glutamate Receptor–T Cell Receptor Signaling Potentiates Full CD8+ T Cell Activation and Effector Function in Tumor Immunity, *iScience*, 2025, **28**(10), 112772, DOI: 10.1016/j.isci.2025.112772.
21 B. G. Kornreich, The Patch Clamp Technique: Principles and Technical Considerations, *J. Vet. Cardiol.*, 2007, **9**(1), 25–37, DOI: 10.1016/j.jvc.2007.02.001.

22 S. G. Cull-Candy and M. M. Usowicz, Patch-Clamp Recording from Single Glutamate-Receptor Channels, *Trends Pharmacol. Sci.*, 1987, **8**(6), 218–224, DOI: 10.1016/0165-6147(87)90066-6.

23 M.-R. Ghovanloo, S. D. Dib-Hajj and S. G. Waxman, The Evolution of Patch-Clamp Electrophysiology: Robotic, Multiplex, and Dynamic, *Mol. Pharmacol.*, 2025, **107**, 100001, DOI: 10.1124/molpharm.124.000954.

24 J. S. Marvin, B. G. Borghuis, L. Tian, J. Cichon, M. T. Harnett, J. Akerboom, A. Gordus, S. L. Renninger, T.-W. Chen, C. I. Bargmann, M. B. Orger, E. R. Schreiter, J. B. Demb, W.-B. Gan, S. A. Hires and L. L. Looger, An Optimized Fluorescent Probe for Visualizing Glutamate Neurotransmission, *Nat. Methods*, 2013, **10**(2), 162–170, DOI: 10.1038/nmeth.2333.

25 J. S. Marvin, B. Scholl, D. E. Wilson, K. Podgorski, A. Kazemipour, J. A. Müeller, S. Schoch-McGovern, F. J. Urra Quiroz, N. Rebola, H. Bao, J. P. Little, A. N. Tkachuk, A. W. Hantman, S. S.-H. Wang, E. R. Chapman, D. Dietrich, D. A. DiGregorio, D. Fitzpatrick and L. L. Looger, Stability, Affinity and Chromatic Variants of the Glutamate Sensor iGluSnFR, *Nat. Methods*, 2017, **15**(11), 936–939, DOI: 10.1038/s41592-018-0171-3.

26 T. P. Jensen, K. Zheng, N. Cole, J. S. Marvin, L. L. Looger and D. A. Rusakov, Multiplex Imaging Relates Quantal Glutamate Release to Presynaptic Ca2+ Homeostasis at Multiple Synapses In Situ, *Nat. Commun.*, 2019, **10**(1), 1414, DOI: 10.1038/s41467-019-09216-8.

27 E. C. Wright, E. Scott and L. Tian, Applications of Functional Neurotransmitter Release Imaging with Genetically Encoded Sensors in Psychiatric Research, *Neuropsychopharmacology*, 2025, **50**(1), 269–273, DOI: 10.1038/s41386-024-01903-5.

28 Y. Wang, D. Mishra, J. Bergman, J. D. Keighron, K. P. Skibicka and A.-S. Cans, Ultrafast Glutamate Biosensor Recordings in Brain Slices Reveal Complex Single Exocytosis Transients, *ACS Chem. Neurosci.*, 2019, **10**(3), 1744–1752, DOI: 10.1021/acschemneuro.8b00624.

29 Y. Wang, H. Fathali, D. Mishra, T. Olsson, J. D. Keighron, K. P. Skibicka and A.-S. Cans, Counting the Number of Glutamate Molecules in Single Synaptic Vesicles, *J. Am. Chem. Soc.*, 2019, **141**(44), 17507–17511, DOI: 10.1021/jacs.9b09414.

30 Q. Wang, C. Yang, S. Chen and J. Li, Miniaturized Electrochemical Sensing Platforms for Quantitative Monitoring of Glutamate Dynamics in the Central Nervous System, *Angew. Chem., Int. Ed.*, 2024, **63**(34), e202406867, DOI: 10.1002/anie.202406867.

31 J. J. Burmeister, D. A. Price, F. Pomerleau, P. Huettl, J. E. Quintero and G. A. Gerhardt, Challenges of Simultaneous Measurements of Brain Extracellular GABA and Glutamate In Vivo Using Enzyme-Coated Microelectrode Arrays, *J. Neurosci. Methods*, 2020, **329**, 108435, DOI: 10.1016/j.jneumeth.2019.108435.

32 B. E. K. Swamy and B. J. Venton, Subsecond Detection of Physiological Adenosine Concentrations Using Fast-Scan Cyclic Voltammetry, *Anal. Chem.*, 2007, **79**(2), 744–750, DOI: 10.1021/ac061820i.

33 D. L. Robinson, B. J. Venton, M. L. A. V. Heien and R. M. Wightman, Detecting Subsecond Dopamine Release with Fast-Scan Cyclic Voltammetry in Vivo, *Clin. Chem.*, 2003, **49**(10), 1763–1773, DOI: 10.1373/49.10.1763.

34 K. A. White and B. N. Kim, Quantifying Neurotransmitter Secretion at Single-Vesicle Resolution Using High-Density Complementary Metal–Oxide–Semiconductor Electrode Array, *Nat. Commun.*, 2021, **12**(1), 431, DOI: 10.1038/s41467-020-20267-0.

35 J. Schultz, Z. Uddin, G. Singh and M. M. R. Howlader, Glutamate Sensing in Biofluids: Recent Advances and Research Challenges of Electrochemical Sensors, *Analyst*, 2020, **145**(2), 321–347, DOI: 10.1039/C9AN01609K.

36 H. M. N. Ahmad, B. Si, G. Dutta, J. R. Csoros, W. R. Seitz and E. Song, Non-Enzymatic Electrochemical Detection Of Glutamate Using Templated Polymer-Based Target Receptors, in *2019 20th International Conference on Solid-State Sensors, Actuators and Microsystems & Eurosensors XXXIII (Transducers & Eurosensors XXXIII)*, IEEE, Berlin, Germany, 2019, pp. 613–616. DOI: 10.1109/Transducers.2019.8808688.

37 H. M. N. Ahmad, G. Dutta, J. Csoros, B. Si, R. Yang, J. M. Halpern, W. R. Seitz and E. Song, Stimuli-Responsive Templated Polymer as a Target Receptor for a Conformation-Based Electrochemical Sensing Platform, *ACS Appl. Polym. Mater.*, 2021, **3**(1), 329–341, DOI: 10.1021/acsapm.0c01120.

38 L. Ahmadian-Alam, A. Andrade and E. Song, Electrochemical Detection of Glutamate and Histamine Using Redox-Labeled Stimuli-Responsive Polymer as a Synthetic Target Receptor, *ACS Appl. Polym. Mater.*, 2024, **6**(10), 5630–5641, DOI: 10.1021/acsapm.4c00121.

39 N. Arroyo-Currás, J. Somerson, P. A. Vieira, K. L. Ploense, T. E. Kippin and K. W. Plaxco, Real-Time Measurement of Small Molecules Directly in Awake, Ambulatory Animals, *Proc. Natl. Acad. Sci. U. S. A.*, 2017, **114**(4), 645–650, DOI: 10.1073/pnas.1613458114.

40 P. Dauphin-Ducharme, K. Yang, N. Arroyo-Currás, K. L. Ploense, Y. Zhang, J. Gerson, M. Kurnik, T. E. Kippin, M. N. Stojanovic and K. W. Plaxco, Electrochemical Aptamer-Based Sensors for Improved Therapeutic Drug Monitoring and High-Precision, Feedback-Controlled Drug Delivery, *ACS Sens.*, 2019, **4**(10), 2832–2837, DOI: 10.1021/acssensors.9b01616.

41 B. S. Ferguson, D. A. Hoggarth, D. Maliniak, K. Ploense, R. J. White, N. Woodward, K. Hsieh, A. J. Bonham, M. Eisenstein, T. E. Kippin, K. W. Plaxco and H. T. Soh, Real-Time, Aptamer-Based Tracking of Circulating Therapeutic Agents in Living Animals, *Sci. Transl. Med.*, 2013, **5**(213), 213ra165, DOI: 10.1126/scitranslmed.3007095.

42 P. L. Mage, B. S. Ferguson, D. Maliniak, K. L. Ploense, T. E. Kippin and H. T. Soh, Closed-Loop Control of Circulating Drug Levels in Live Animals, *Nat. Biomed. Eng.*, 2017, **1**(5), 0070, DOI: 10.1038/s41551-017-0070.

43 H. M. N. Ahmad, A. Andrade and E. Song, Continuous Real-Time Detection of Serotonin Using an Aptamer-Based Electrochemical Biosensor, *Biosensors*, 2023, **13**(11), 983, DOI: 10.3390/bios13110983.

44 O. Alkhamis, J. Canoura, H. Yu, Y. Liu and Y. Xiao, Innovative Engineering and Sensing Strategies for Aptamer-Based Small-Molecule Detection, *TrAC, Trends Anal. Chem.*, 2019, **121**, 115699, DOI: 10.1016/j.trac.2019.115699.

45 R. Kou, J. Zhang, T. Wang and G. Liu, Interactions between Polyelectrolyte Brushes and Hofmeister Ions: Chaotropes versus Kosmotropes, *Langmuir*, 2015, **31**(38), 10461–10468, DOI: 10.1021/acs.langmuir.5b02698.

46 N. Just and S. Sonnay, Investigating the Role of Glutamate and GABA in the Modulation of Transthalamic Activity: A Combined fMRI-fMRS Study, *Front. Physiol.*, 2017, **8**, 30, DOI: 10.3389/fphys.2017.00030.

47 E. Thormann, On Understanding of the Hofmeister Effect: How Addition of Salt Alters the Stability of Temperature Responsive Polymers in Aqueous Solutions, *RSC Adv.*, 2012, **2**(22), 8297–8305, DOI: 10.1039/C2RA20164J.

48 Y. Zhang, S. Furyk, D. E. Bergbreiter and P. S. Cremer, Specific Ion Effects on the Water Solubility of Macromolecules: PNIPAM and the Hofmeister Series, *J. Am. Chem. Soc.*, 2005, **127**(41), 14505–14510, DOI: 10.1021/ja0546424.

49 Y.-C. Tsai, W.-Y. Weng, Y.-T. Yeh and J.-C. Chien, Dual-Aptamer Drift Canceling Techniques to Improve Long-Term Stability of Real-Time Structure-Switching Aptasensors, *ACS Sens.*, 2023, **8**(9), 3380–3388, DOI: 10.1021/acssensors.3c00509.

50 M. G. Langer and A. Koitschev, The Biophysics of Sensory Cells of the Inner Ear Examined by Atomic Force Microscopy and Patch Clamp, in *Methods in Cell Biology*, Elsevier, 2002, vol. 68, pp. 141–169. DOI: 10.1016/S0091-679X(02)68008-2.

51 S. H. F. Pedersen, *Reviews of Physiology, Biochemistry and Pharmacology*, Springer Nature Switzerland, Cham, 2023, vol. 186. DOI: 10.1007/978-3-031-25628-8.

52 N. D. Hershey, P. Popov, N. M. Oliver, C. E. Dugan and R. T. Kennedy, Detection of Neuronal Glutamate in Brain Extracellular Space In Vivo Using Microdialysis and Metabolic Labeling with Glutamine, *ACS Chem. Neurosci.*, 2025, **16**(17), 3398–3409, DOI: 10.1021/acschemneuro.5c00518.

53 M. König, A. Thinnes and J. Klein, Microdialysis and Its Use in Behavioural Studies: Focus on Acetylcholine, *J. Neurosci. Methods*, 2018, **300**, 206–215, DOI: 10.1016/j.jneumeth.2017.08.013.

54 R. T. Kennedy, C. J. Watson, W. E. Haskins, D. H. Powell and R. E. Strecker, In Vivo Neurochemical Monitoring by Microdialysis and Capillary Separations, *Curr. Opin. Chem. Biol.*, 2002, **6**(5), 659–665, DOI: 10.1016/S1367-5931(02)00373-3.

55 M. Perry, Q. Li and R. T. Kennedy, Review of Recent Advances in Analytical Techniques for the Determination of Neurotransmitters, *Anal. Chim. Acta*, 2009, **653**(1), 1–22, DOI: 10.1016/j.aca.2009.08.038.

56 R. Divya Mohan, S. Rajendrachari, H. De Araujo Silva Neto, A. Santhy and R. Rejithamol, Exploration and Advances in Enzymatic Electrochemical Biosensors for in Vivo Detection of Brain Glutamate, *Bioelectrochemistry*, 2026, **168**, 109161, DOI: 10.1016/j.bioelechem.2025.109161.

57 Y. Xie, A. W. Chan, A. McGirr, S. Xue, D. Xiao, H. Zeng and T. H. Murphy, Resolution of High-Frequency Mesoscale Intracortical Maps Using the Genetically Encoded Glutamate Sensor iGluSnFR, *J. Neurosci.*, 2016, **36**(4), 1261–1272, DOI: 10.1523/JNEUROSCI.2744-15.2016.

58 X. Zhong, H. Gu, J. Lim, P. Zhang, G. Wang, K. Zhang and X. Li, Genetically Encoded Sensors Illuminate in Vivo Detection for Neurotransmission: Development, Application, and Optimization Strategies, *IBRO Neurosci. Rep.*, 2025, **18**, 476–490, DOI: 10.1016/j.ibneur.2025.03.003.

59 Y. Yang, B. Li and Y. Li, Genetically Encoded Sensors for the In Vivo Detection of Neurochemical Dynamics, *Annu. Rev. Anal. Chem.*, 2024, **17**(1), 367–392, DOI: 10.1146/annurev-anchem-061522-044819.

60 J. Day-Cooney, R. Dalangin, H. Zhong and T. Mao, Genetically Encoded Fluorescent Sensors for Imaging Neuronal Dynamics in Vivo, *J. Neurochem.*, 2023, **164**(3), 284–308, DOI: 10.1111/jnc.15608.